

Article

## Preparation and Properties of Cellulose Laurate (CL)/Starch Nanocrystals Acetate (SNA) Bio-nanocomposites

Feng-Yuan Huang <sup>1,2,\*</sup>, Xiao-Jie Wu <sup>2</sup>, Yan Yu <sup>2</sup> and Yan-Hua Lu <sup>1,\*</sup>

<sup>1</sup> Key Lab of Functional Textile Materials, Eastern Liaoning University, Dandong, 118003, Liaoning, China

<sup>2</sup> School of Chemical Engineering, Eastern Liaoning University, Dandong, 118003, Liaoning, China; E-Mails: ht51888@163.com (X.J.W.); ldxytyy@163.com (Y.Y.)

\* Authors to whom correspondence should be addressed;

E-Mails: huangfengyuan@hotmail.com (F.Y.H.); yanhua00\_lu@hotmail.com (Y.H.L.);  
Tel.: +86-415-378-9735; Fax: +86-415-378-9981.

Academic Editor: Lloyd M. Robeson

Received: 13 June 2015 / Accepted: 8 July 2015 / Published: 14 July 2015

---

**Abstract:** In the present paper, a series of totally novel bio-nanocomposite films from cellulose laurate (CL) and starch nanocrystals acetate (SNA) were fabricated, and the properties of nanocomposite films were investigated in detail. SNA was obtained by modifying starch nanocrystals (SNs) produced by sulfuric acid hydrolysis of corn starch with acetic anhydride. The favorable dispersity of SNA in chloroform made it ready to convert into nanocomposite films with CL via casting/evaporation method. The transmittance, thermal behavior, mechanical properties, barrier properties and hydrophobicity of CL/SNA nanocomposite films were investigated with UV-vis spectrophotometer, simultaneous thermal analyzer (STA), universal tensile tester/dynamic thermomechanical analysis (DMA), water vapor permeation meter/oxygen permeability tester, and contact angle tester, respectively. The transmittance of nanocomposite films decreased with the increase of SNA content. Thermogravimetric analysis (TGA) results showed that the introduction of SNA into CL matrix did not severely decrease the thermal behavior of CL/SNA nanocomposites. Moreover, non-linear and linear mechanical analysis reflected the enhancement of SNA. At lower contents of SNA (<5.0 wt%), the values of Young's modulus, tensile strength and the elongation at break of nanocomposite films were comparable with those of neat CL. However, with the increase of SNA, the Young's modulus and tensile strength were improved significantly and were accompanied by the decreased elongation at break. The water vapor

permeability (WVP) and oxygen permeability ( $P_{O_2}$ ) of CL/SNA nanocomposite films were significantly improved by the addition of SNA.

**Keywords:** cellulose laurate (CL); starch nanocrystals acetate (SNA); CL/SNA bio-nanocomposite; tensile property; barrier property

---

## 1. Introduction

Starch and cellulose are two important natural, renewable, biodegradable polymers, and are regarded as potential alternative candidates for the synthesized polymers derived from petroleum resources. Cellulose acetate (CA), as one of the most common and important short chain cellulose esters, has been used as thermoplastic plastic in packing, textile, building and plastic industries [1]. However, the shortage of CA is distinct for the narrow temperature window between melting temperature and decomposition. Long chain fatty acid cellulose esters (FACEs) were considered to cover the shortages of short-chain cellulose esters, and identified as potential biodegradable plastics due to the enzymatically labile ester bond and the natural abundance of both cellulose and fatty acids [2,3]. FACEs are of particular interest for their good biocompatibility and nontoxicity [4–6]. Moreover, the applications of FACEs have attracted more and more attention. Their mechanical and thermal properties were investigated extensively by many authors [7,8]. To meet the demand of applications of FACEs, several paths for the synthesis of FACEs had been developed [9]. However, the properties of FACEs cannot meet all the demands for the usage as materials, especially for their relative low mechanical strength.

To enhance the strength, fabrication of polymers based nanocomposites with nanofillers is an effective route. Compared to conventional composites, nanocomposites show unique properties even at low filler content [10]. Stiffness, strength, toughness, thermal stability, and even barrier properties of the pure polymer matrix, can be improved with nanofillers [11]. Furthermore, because the particles are smaller than the wavelength of visual light, nanofillers did not affect the transmittance of the polymer matrix. With the increase of environmental issues, organic nanoparticles from renewable resources for new barrier bio-based packaging are receiving more and more attention. Starch nanocrystals (SNs), obtained by hydrolyzing various starch, are receiving a significant amount of attention because of the abundant availability of starch, low cost, renewability, biocompatibility, biodegradability, and non-toxicity [12,13]. A large number of polymers could be enhanced with SNs, such as poly (styrene-*co*-butyl acrylate) [14], natural rubber [15], and some environment-friendly polymers [16–22]. It was interesting to know that the content of SNs in different polymer matrices bring out quite different fractions. Natural rubber reinforced with 10 wt% waxy maize SNs showed remarkable barrier properties of water vapor and oxygen [15]. Waterborne polyurethane filled with 5 wt% SNs had the highest tensile strength, increased Young's modulus, and an increasing elongation at break [16]. The content of SNs in thermoplastic starch even attained 25% [19]. To our knowledge, there is no information on nanocomposites of FACEs enhanced with nanofillers.

The work presented here focuses on the properties of FACE-based green bio-nanocomposites with SNA enforcement. In order to elaborate the comprehensive properties of CL/SNA nanocomposites,

the transmittance, thermal, mechanical, and barrier properties of CL/SNA nanocomposite were investigated in detail.

## 2. Experimental Section

### 2.1. Materials

The cellulose used was microcrystal cellulose (MCC) powder (OurChem, DP = 235). Special grade trifluoroacetic anhydride (TFAA) and lauric acid were used for the acylation of cellulose. Corn starch (S) was used as supplied from Sinopharm Chemical Reagent Co., Ltd, China. Reagent grade sulfuric acid, sodium hydroxide, acetic anhydride, chloroform, and other reagents were used without being further purified.

### 2.2. Fabrication of SNs

SNs were prepared by acid hydrolysis of corn starch according to references [23,24]. Corn starch powders were mixed with 3.16 M H<sub>2</sub>SO<sub>4</sub> solution at a starch concentration of 20 wt% in a flask. The suspensions were then continuously stirred at 100 rpm under 40 °C. After five days of hydrolysis, the suspensions were washed by successive centrifugations in distilled water until neutrality was achieved. The SN precipitate was ultrasonically homogenized in an aqueous solution and then the SN suspension was freeze-dried under vacuum.

### 2.3. Synthesis of SNA

SNs (2.0 g), acetic anhydride (18 mL) and sodium hydroxide 50 wt% solution (5.0 mL) were mixed and refluxed for 15 min at 150 °C. The reaction mixture was added to cold water to precipitate, and the product was collected by normal filtration, washed repeatedly with water and freeze-dried under vacuum. Then, SNA was prepared.

### 2.4. Preparation of CL/SNA Nanocomposite Films

CL was synthesized following the method described in reference [2] with some modifications. TFAA and lauric acid (molar ratio of fatty acid to TFAA was 1.1:1.0) were mixed together in a 250 mL three-neck flask equipped with a condenser and stirred mildly at 50 °C for 20 min to form the mixed acid anhydride. Pre-dried MCC powder (molar ratio of TFAA to MCC was 3:1) was added to this solution and stirred mildly at 50 °C for 5 h. The reaction mixtures were poured into an excess amount of ethanol, and the precipitates were filtered and washed with methanol (50 mL per gram of MCC) three times at 60 °C. Finally, the polymers were dried at 50 °C for 24 h under vacuum to yield products. The degree of substitution (DS) of CL was 2.68 according to <sup>1</sup>H NMR.

The nanocomposite films were manufactured by casting/evaporation technique using chloroform as solvent. The desired amount of SNA was dispersed in chloroform without any other reagents by vigorously stirring and then by ultrasonication for 30 min to obtain a homogeneous suspension. CL was dissolved in the SNA suspension with vigorous stirring for 1 h and then ultrasonicated for 5 min to achieve a dispersion of SNA in the matrix. The concentration of CL in chloroform was 0.5 g/g. Subsequently, the mixture was cast into a Petri disk and the solvent was evaporated at ambient temperature

for 24 h. In order to evaporate chloroform completely, the disk was removed to an oven at 50 °C under vacuum for another 4 h. The CL/SNA nanocomposite films, with 1.0, 3.0, 5.0, 7.0, and 10 wt% of SNA, were labeled as CL/SNA01, CL/SNA03, CL/SNA05, CL/SNA07, and CL/SNA10, respectively. The thickness of the obtained films was about 120–140 µm.

CL film was fabricated by casting/evaporation technique using chloroform as solvent in a similar procedure as preparation of CL/SNA nanocomposite films.

## 2.5. Analytical Methods

### 2.5.1. Fourier Transform Infrared Spectrometer (FTIR)

FTIR spectra for all samples were measured on a PerkinElmer Spectrum 100 (PerkinElmer, Waltham, USA) using the KBr pellet technique for all samples. KBr tablets were dried at 105 °C for 1 h to remove moisture prior to the measurement.

### 2.5.2. Characterization of SNs Particles

Particles size and particle distribution of SN were measured on a Zetasizer Nano ZSP (Malvern Instruments Ltd., Malvern, UK). SNs particles (0.1 g) were added into 10 mL deionized water to form suspension in the concentration of SNs about 0.01 g/mL, and then 1.5 mL liquid was added to the sample cell for the measurement.

### 2.5.3. Light Transmittance of CL/SNA Nanocomposite Films

Light transmittance of the films was measured using an SP-721E UV-vis spectrophotometer (Spectrum Instrument Co., Ltd., Shanghai, China). Transmission spectra of the films were recorded using air as reference.

### 2.5.4. Thermogravimetric Analysis

Thermogravimetric analysis for all samples was conducted on a STA (449F TG/DSC, NETZSCH, Selb, Germany). The samples were heated from 30 °C till 600 °C at the heating rate of 10 °C/min. All samples were in a 50 mL/min flow of Ar.

### 2.5.5. Tensile Analysis

The tensile strength and elongation at break of the films were measured on a universal tensile tester (TS7104, SANS, Shenzhen, China) according to GB/T 1040.3-2006 at a speed of 5.0 mm/min. All of the tests were performed at 23 °C and 40% relative humidity (RH). The specimens were in a rectangular shape with a dimension of 60 mm × 10 mm × (0.12–0.24) mm. The length between two grips was set as 30 mm.

### 2.5.6. Dynamic Mechanical Analysis (DMA)

DMA measurements were performed on a NETZSCH DMA 242 apparatus (NETZSCH, Selb, Germany) operating in tensile mode at a frequency of 1 Hz over the temperature range  $-55\text{ }^{\circ}\text{C} < T < 150\text{ }^{\circ}\text{C}$  in a heating rate of  $5\text{ }^{\circ}\text{C}/\text{min}$ . Specimens with gauge width and length  $5\text{ mm} \times 24\text{ mm}$  were cut out from the CL or CL/SNA casting films.

### 2.5.7. Contact Angles Measurements

Contact angles of on film surfaces for water droplets were measured at  $23\text{ }^{\circ}\text{C}$  and 50% Relative humidity (RH) on contact angle instrument (XG-CAMA, Xuanyichuangyi Industrial Equipment Co., Ltd., Shanghai, China). A water droplet of  $4\text{ }\mu\text{L}$  was dropped onto the films and the images were taken after 15 s.

### 2.5.8. Barrier Properties Measurements

The oxygen permeability of the films was determined at  $23\text{ }^{\circ}\text{C}$  and 40% RH using a VAC-V2 (Labthink, Jinan, China) under standard conditions (GB/T 1038-2000).

$$P_{O_2} = \frac{\Delta p \cdot V \cdot T_0 \cdot D}{\Delta t \cdot S \cdot p_0 \cdot T \cdot (p_1 - p_2)} \quad (1)$$

where  $P_{O_2}$ , Oxygen permeability in  $\text{mL} \cdot \text{cm} \cdot \text{cm}^{-2} \cdot \text{s} \cdot \text{Pa}$ ;  $\Delta p/\Delta t$ , The arithmetic average gas pressure changing value in low pressure chamber within unit time in  $\text{Pa}/\text{s}$ ;  $T_0$ ,  $273.15\text{ K}$ ;  $T$ , Temperature for testing in  $\text{K}$ ;  $p_0$ ,  $1.0133 \times 10^5\text{ Pa}$ ;  $V$ , Volume of lower pressure chamber in  $\text{mL}$ ;  $S$ , Area of sample in  $\text{cm}^2$ ;  $(p_1 - p_2)$ , Partial pressure difference across the films in  $\text{Pa}$ .

Water vapor permeability (WVP) was determined gravimetrically according to the standard method GB 1037-88 with moisture analyzer (STW-801L, Labstone, Guangzhou, China). The films were fixed on top of test cells containing a desiccant (Anhydride Calcium Chloride,  $\text{CaCl}_2$ ). Test cells then were placed in a relative humidity chamber with controlled temperature ( $23\text{ }^{\circ}\text{C}$ ) and relative humidity (90% RH). After steady-state conditions were reached, the weight of test cells was measured after 24 h. All the tests were performed in triplicate at 1 atm and WVP was reported as the average of these three values. The WVP was determined as:

$$WVP = \frac{\Delta m \cdot d}{A \cdot t \cdot \Delta p} \quad (2)$$

where WVP, Water vapor permeability in  $\text{g} \cdot \text{cm} \cdot \text{cm}^{-2} \cdot \text{s}^{-1} \cdot \text{Pa}^{-1}$ ;  $\Delta m$ , Weight change in  $\text{g}$ ;  $\Delta t$ , The exposure time in the chamber in  $\text{s}$ ;  $A$ , Test area in  $\text{cm}^2$ ;  $d$ , Thickness of film in  $\text{cm}$ ;  $\Delta p$ , Partial pressure difference across the films in  $\text{Pa}$ .

## 3. Results and Discussion

### 3.1. Synthesis and Characterization of SNA

From the molecular structure of SNs point of view, the hydrophilic nature of SNs made it disperse well in polar solvents (e.g., Water) rather than in non-polar solvents (e.g., Chloroform). However, the neat CL dissolved in chloroform readily. Thus, it was necessary to modify SNs further and to obtain

well-dispersed derivative in chloroform. Starch nanocrystals acetate (SNA), via acylation of SNs with acetic anhydride, can meet this requirement.

### 3.1.1. FTIR

Figure 1 shows the FTIR spectra of the S, SN and SNA powders. There was no distinct difference between spectrum of S and SN, which indicated that the chemical structure of S and SN had no substantial change during fabrication of SN from S. However, there is a new small distinct peak located at  $1736\text{ cm}^{-1}$  in the spectrum of SNA, which is attributed to the C=O stretching of the carbonyl group in the ester bond. This indicated that some of hydroxyl groups have been substituted by acetate. However, the absorption above  $3000\text{ cm}^{-1}$ , assigned to O–H stretching, did not decrease observably. This suggested that the degree of substitution was relatively low, and it was enough to improve the dispersity of SNA in chloroform, which was confirmed in the next section.

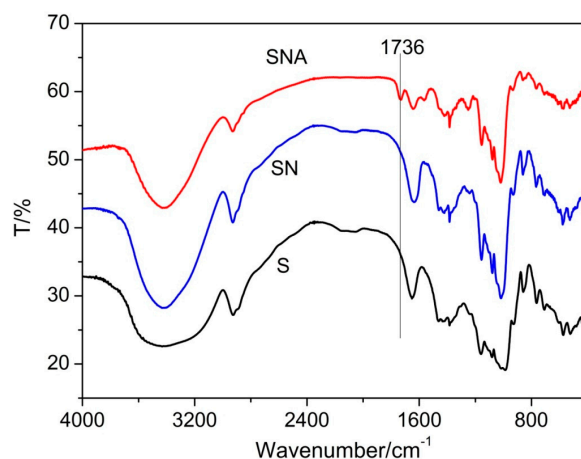


**Figure 1.** FTIR spectra of S, SN and SNA.

### 3.1.2. Dispersion in Different Solvents and Particles Distribution of SNs and SNA

The dispersion states of SN and SNA in water and chloroform are shown in Figure 2. SN particles dispersed well in water, but aggregated in chloroform for their nature hydrophilic characteristics. On the contrary, SNA particles dispersed uniformly in chloroform but not well in water. The dispersion of SNA in chloroform could guarantee the homogeneous composition of CL/SNA nanocomposite films.

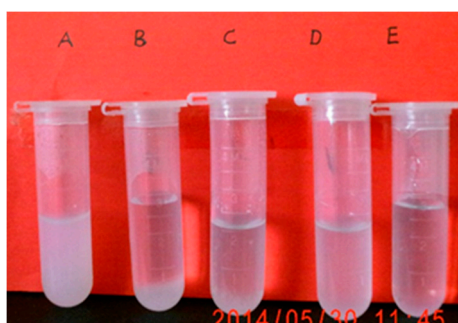


**Figure 2.** Photograph of dispersion of SN in water (A) and in Chloroform (C); SNA in DI water (B) and in Chloroform (D); for comparison DI water was shown as (E).

Because SN could disperse uniformly in water, it was possible to determine their particles' size and distribution in DI water. Figure 3 shows the results of particle distribution of SN in DI water. Most of SN particles' radius was in the range of 25–35 nm (the fraction was >50%). Additionally, all of the diameter was in the range of 40–110 nm. The particle size of SN prepared in the paper from corn starch was in good agreement with the previous results [23,25].

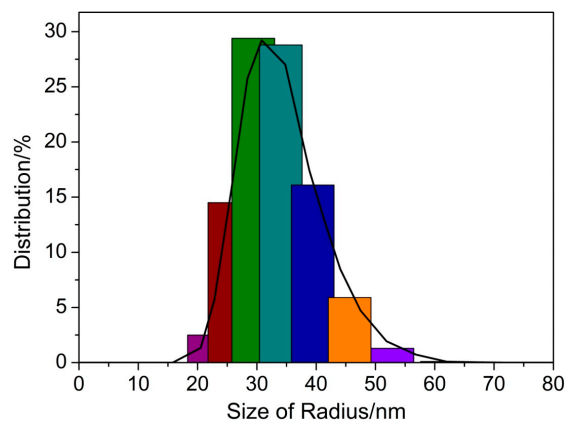


**Figure 3.** SN particles size and their distribution.

### 3.2. Properties of CL/SNA Nanocomposite Films

#### 3.2.1. Light Transmittance of CL/SNA Nanocomposite Films

The UV-vis transmittance spectra of the films at visible wavelength range of 400–800 nm are shown in Figure 4. The transmittance of all nanocomposite films at any wave length within 400–800 nm was more than 50%, except for 7.0% and 10% SNA loaded. The transmittance of nanocomposite films with 1.0, 3.0, 5.0, 7.0 and 10.0 wt% SNA at 400 nm were 68.2%, 65.7%, 55.7%, 50.0% and 46.8%, respectively, whereas 69.6% for a neat CL film. The transmittance of CL/SNA10 was a little higher than 50% at 800 nm; however, the value decreased to 46.8% at 400 nm. These results indicated that the increase of SNA content may affect the dispersion state of SNA in CL matrix, further deteriorating the transparency of CL film. The similar results were reported by Nogi *et al.*, when they investigated the transmittance of neat cellulose nanocrystal films [26,27]. The decreased transmittance with increase of SNA content in CL matrix can be explained by the formation of fewer agglomerates in the nanocomposite and light scattering at interface between SNA-rich and CL-rich phases.

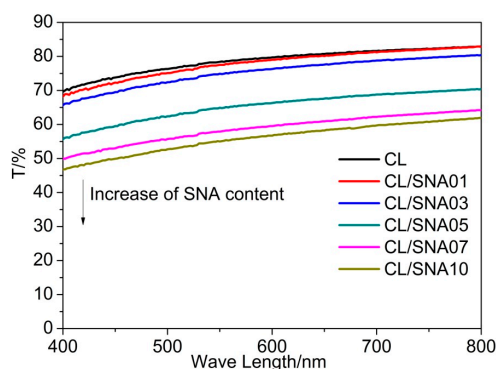


**Figure 4.** Transmittance of CL film and CL/SNA nanocomposite films.

### 3.2.2. Thermogravimetric Analysis (TG)

TG and derivative thermogravimetric analysis DTG curves of CL/SNA, SNA, and neat CL are shown in Figure 5. From Figure 5, SNA displayed two thermal loss behaviors at *ca.* 100 °C and 319 °C, respectively. The first loss behavior was belonging to dehydration of adsorbed water, which indicated that SNA has a certain degree of hydrophilicity. FTIR results had confirmed that the DS of SNA was low, and there are a lot of OH groups on SNA. The second loss behavior began from *ca.* 250 °C and an incipient temperature at *ca.* 319 °C, which assigned to the thermal decomposition of SNA. For neat CL, the beginning decomposition temperature was about 300 °C and a peak temperature at *ca.* 375 °C. However, by comparison with DTG curves of SNA and neat CL, it was found the decomposition behavior of CL/SNA nanocomposites was different from that of SNA and CL. As seen in Figure 5b, all the CL/SNA nanocomposites displayed two DTG peaks, ~319 °C and ~375 °C, but they did not show a dehydration peak at *ca.* ~100 °C. It was safe to say that the SNA loaded in CL/SNA nanocomposites results in the lower peak (~319 °C). After the decomposition of SNA, the CL in nanocomposites began to decompose at a higher temperature. The temperatures at the maximum degradation rate of CL/SNA nanocomposites were almost the same as the neat CL, which indicated that the load of SNA in CL only slightly affected the thermal behavior of CL/SNA nanocomposites. Additionally, the final char percentage increased with the increase of SNA content.

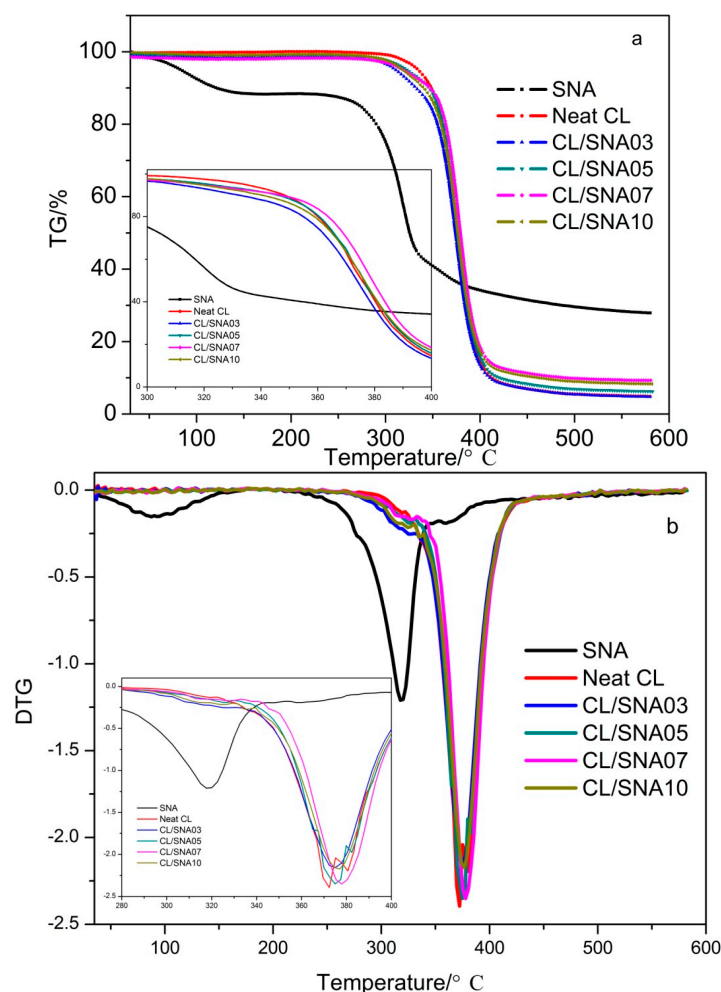


**Figure 5.** TG (a) and DTG (b) of CL/SNA, SNA, and CL.

### 3.2.3. Mechanical Properties

The SNA as a reinforcing phase in the CL matrix has been evaluated from a mechanical point of view, both in the non-linear (tensile tests) and linear (DMA) range.

#### Tensile Tests

Typical stress–strain curves of the CL/SNA nanocomposite films and neat CL under uniaxial tensile at 23 °C are shown in Figure 6. Three measurements for each sample were carried out, and the average values of the tensile strength ( $\sigma_b$ ), Young's modulus (E) and elongation at break ( $\epsilon_b$ ) were calculated and summarized in Table 1.

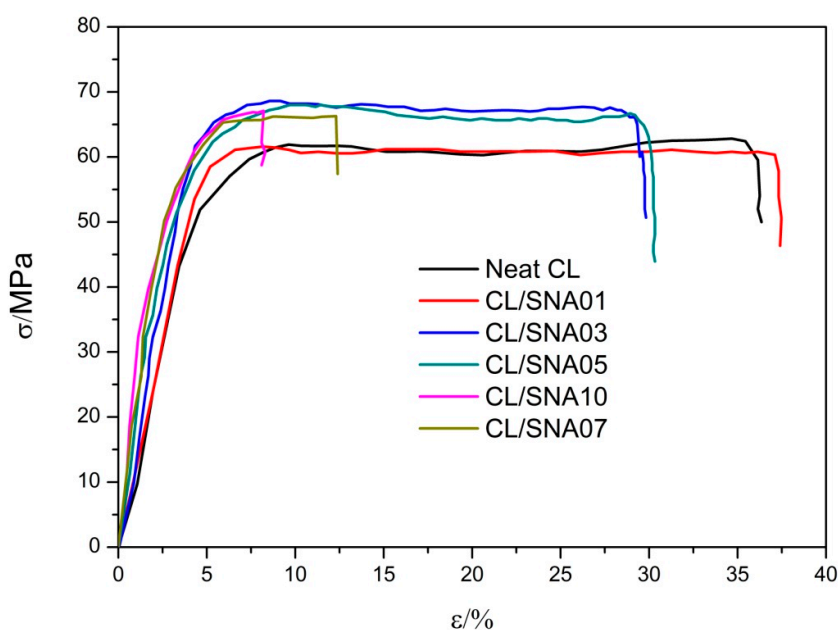


**Figure 6.** Typical stress-strain curves of the CL/SNA nanocomposite films under uniaxial tensile at 23 °C.

Table 1 shows the evolution of the  $\sigma_b$ , E and  $\epsilon_b$  as a function of SNA content in CL/SNA nanocomposite films. For neat CL film, the  $\sigma_b$ , E and  $\epsilon_b$  were 59.5 MPa, 200.08 MPa and 36.5%, respectively. These values were in consistent with the other authors' results [8]. Compared with neat CL film, CL/SNA01 with lower SNA loaded, showed comparable  $\sigma_b$  and  $\epsilon_b$ , whereas higher E. With the increase of SNA content, the enhancement of  $\sigma_b$  and E was based on the expense of elongation at break. For instance, the  $\sigma_b$  and E of CL/SNA05 increased to 65.4 MPa and 330.09 MPa, respectively, and the  $\epsilon_b$  decreased to 28.3%. This result was different from the previous reports about cellulose ester based nanocomposites. Yang *et al.* found that these values were improved to varying degrees, when they investigated properties of cellulose acetate modified with cellulose nanocrystals [28]. The difference might result from the different appearance of SNs and cellulose nanocrystals. For most cellulose nanocrystals, the L/D ratio was more than 20 [29]. However, the L/D ratio for SNs was far smaller than the former value [10], and the SNs looked like round particles and a decrease of elongation with the increase of SNA in the matrix was observed. Furthermore, higher SNA loading level resulted in a decrease of the elongation due to the self-aggregation of SNA, and similar results were reported by other authors [16,21,22,30]. The above results indicated that there might be an underlying structure whose formation controls the

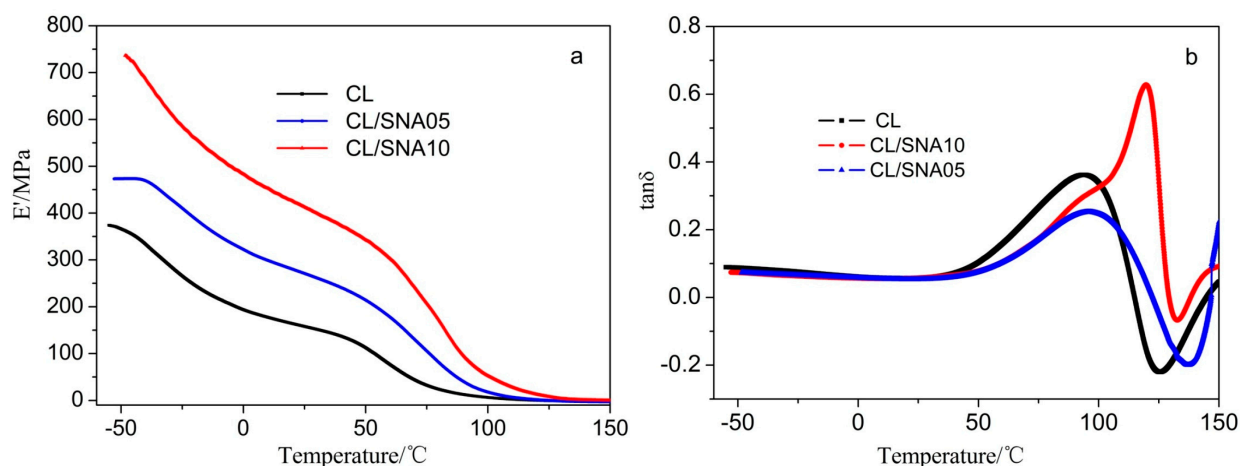
tensile performance evolution with SNA content. The reinforcing effect of SNA may ascribe to the formation of a hydrogen bonded percolating filler network above a given SNA content corresponding to the percolation threshold. However, as described by Dufresne *et al.*, the percolation theory is difficult to prove for polymer matrix with starch nanocrystals because the connecting particles should be starch clusters or aggregates with ill-defined size and geometry [10].

**Table 1.** Tensile strength ( $\sigma_b$ ), Young's modulus (E), and elongation at break ( $\epsilon_b$ ) of CL/SNA nanocomposite films under uniaxial tensile at 23 °C. The values correspond to the mean  $\pm$  standard deviation (SD) of three measurements for the same sample.

| Sample   | $\sigma_b$ /MPa  | E/MPa              | $\epsilon_b$ /% |
|----------|------------------|--------------------|-----------------|
| CL       | 59.53 $\pm$ 4.56 | 200.08 $\pm$ 10.27 | 36.5 $\pm$ 2.14 |
| CL/SNA01 | 58.86 $\pm$ 5.71 | 267.77 $\pm$ 14.31 | 37.7 $\pm$ 3.52 |
| CL/SNA03 | 60.02 $\pm$ 6.23 | 310.30 $\pm$ 10.89 | 28.3 $\pm$ 1.89 |
| CL/SNA05 | 65.41 $\pm$ 7.85 | 330.09 $\pm$ 22.14 | 28.5 $\pm$ 3.26 |
| CL/SNA07 | 65.83 $\pm$ 5.34 | 335.49 $\pm$ 19.78 | 11.8 $\pm$ 1.08 |
| CL/SNA10 | 67.17 $\pm$ 2.11 | 338.57 $\pm$ 25.31 | 8.1 $\pm$ 1.13  |

#### Dynamic Mechanical Analysis (DMA)

The evolution of storage modulus  $E'$  and loss factor  $\tan\delta$  as a function of temperature is presented in Figure 7. Figure 7a shows that the neat CL has a storage modulus of 380 MPa at  $-50$  °C. The storage modulus of CL/SNA nanocomposites increased with increasing of SNA contents. All the storage modulus of the nanocomposites were higher than the neat CL in the temperature range from  $-50$  °C to 150 °C. The results indicated that the well-dispersed SNA stiffen the CL matrix. This reinforcing effect of SNA was believed to be attributed to the formation of a percolating starch nanocrystals network through hydrogen linkages between starch nanoparticles clusters [31].



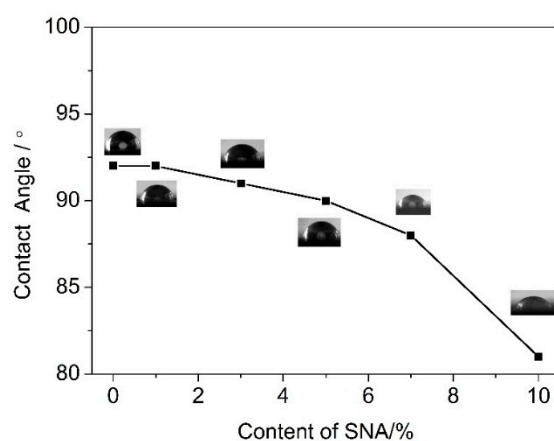
**Figure 7.** Dynamic mechanical response of CL and CL/SNA nanocomposite films as a function of temperature, recorded at 1 Hz frequency (a) storage modulus  $E'$  and (b) loss factor ( $\tan\delta$ ).

Figure 7b presents the variation of  $\tan\delta$  as a function of temperature for the neat CL and CL/SNA nanocomposites. For the neat CL, the shape of  $\tan\delta$  peak suggests that  $T_g$  was about 88 °C, which was

comparable with the  $T_g$  of cellulose tri-laurate reported by Vaca-Garcia *et al.* [32]. The shape of  $\tan\delta$  of CL/SNA05 was the same as CL, and the  $T_g$  value was also nearly the same. However, the  $\tan\delta$  peak of CL/SNA10 displayed two overlapping transitions, the first one at around 88 °C and the second one increased to 118 °C. The first peak assigned to the  $T_g$  transition of CL, the second was attributed to the relaxation transitions of the SNA rich domain, which hindered lateral rearrangements of CL chains and crystallization of CL films with higher SNA content [33,34].

### 3.2.4. Contact Angles of CL/SNA Nanocomposite Films

The change in surface polarity from the CL to CL/SNA nanocomposites was evaluated with static water contact angle measurements (Figure 8). The neat CL film presented a high contact angle value of 92° (which was close to the results from Crépy [8]), as expected due to the hydrophobic character of CL. The contact angles decreased with the increase of SNA contents. However, when the content of SNA increased from 0 wt% to 7.0 wt%, the contact angle decreased by only 6°. With a further increase of content of SNA in CL to 10 wt%, the value decreased rapidly, from 92° to 82°. The dispersion state of SNA in CL may explicate the above results. When small amount of SNA were added, the SNA particles were coated by CL, and SNA were uniformly dispersed in the matrix. Thus, the surface of nanocomposite films was nearly the same as that of the neat CL, and the contact angle changed negligibly (for CL/SNA05, the value was 91°). Whereas, when the content of SNA increased to 10 wt%, some SNA particles were not completely coated by CL, and there were some independent or aggregated SNA particles on the surface of nanocomposite films. Furthermore, due to the low DS of SNA (as discussed in former sections), there was a considerable amount of OH groups on SNA, and moisture absorption of the polar bonds was non-negligible. Thus, the hydrophobicity of CL/SNA nanocomposite films was inferior to that of neat CL, when the SNA content exceeds 5.0 wt%.



**Figure 8.** Static water contact angle for CL and CL/SNA.

### 3.2.5. Barrier Properties of CL/SNA Nanocomposite Films

Oxygen and water vapor permeability (WVP) are two important parameters for packaging materials [35]. Table 2 lists the oxygen and water vapor barrier properties of the CL/SNA nanocomposite films. For neat CL, the WVP and  $P_{O_2}$  was  $8.85 \times 10^{-6} \text{ g} \cdot \text{cm} \cdot \text{cm}^{-2} \cdot \text{s}^{-1} \cdot \text{Pa}^{-1}$  and  $7.08 \times 10^{-14} \text{ mL} \cdot \text{cm} \cdot \text{cm}^{-2} \cdot \text{s}^{-1} \cdot \text{Pa}^{-1}$ , respectively. Both WVP and  $P_{O_2}$  of the CL/SNA composite films decreased for all formulations.

The values decreased to 8.71, 7.34, 7.36, and  $7.08 \times 10^{-11} \text{ g}\cdot\text{cm}\cdot\text{cm}^{-2}\cdot\text{s}^{-1}\cdot\text{Pa}^{-1}$  for the 1.0 wt%, 5.0 wt%, 7.0 wt% and 10 wt% loading of SNA, respectively. With the increase of SNA content,  $P_{O_2}$  reduced by 2%, 8%, 9.5%, and 10.3% for CL/SNA01, CL/SNA05, CL/SNA07 and CL/SNA10, respectively.

**Table 2.** Effects of SNA content on barrier properties of nanocomposite films.

| Sample   | WVP ( $\times 10^{-6} \text{ g}\cdot\text{cm}\cdot\text{cm}^{-2}\cdot\text{s}^{-1}\cdot\text{Pa}^{-1}$ ) | $P_{O_2}$ ( $\times 10^{-14} \text{ mL}\cdot\text{cm}\cdot\text{cm}^{-2}\cdot\text{s}^{-1}\cdot\text{Pa}^{-1}$ ) |
|----------|--|--|
| CL       | $8.85 \pm 0.08$  | $7.08 \pm 0.07$  |
| CL/SNA01 | $8.71 \pm 0.05$  | $6.98 \pm 0.11$  |
| CL/SNA03 | -  | -  |
| CL/SNA05 | $7.34 \pm 0.10$  | $6.52 \pm 0.08$  |
| CL/SNA07 | $7.36 \pm 0.11$  | $6.41 \pm 0.13$  |
| CL/SNA10 | $7.08 \pm 0.06$  | $6.35 \pm 0.05$  |

It was obvious that the barrier properties of the nanocomposite films were significantly improved by the addition of SNA. The similar results were observed by Angellier *et al.*, when they investigated permeability of rubber with waxy maize SNs as nanofillers [15]. Generally, water vapor transmission through a film depends on both diffusivity and solubility of water molecules in the film matrix. At lower SNA contents, the better dispersion and lower aggregation of SNA particles occurred, contributing to generate a tortuous path for the passage of water molecules evoking a decrease in WVP [36]. Thus, the presence of SNA led to the increase of the tortuosity in the CL matrix and slows down water vapor diffusion processes and to a lower WVP. For oxygen, on the one hand, the platelet-like structures of the SNA stand in the way of the oxygen molecules, increasing the tortuosity of the diffusion path. On the other hand, the formation of a hydrogen bonding network between SNA and CL induces an increased residence time of the oxygen molecule and the resulting low permeability, which had been confirmed by Dou *et al.* when they investigated the barrier property of layered double hydroxide/cellulose acetate [37]. The results indicated that improvement in CL/SNA nanocomposite film barrier properties depended on the occurrence of intercalation or exfoliation [38].

#### 4. Conclusions

In the present paper, SNs were obtained by sulfuric acid hydrolysis of corn starch. After surface modification of SNs with acetic anhydride, SNA, which was readily to disperse in chloroform, was attained. CL based bio-nanocomposites with SNA were converted into films using casting/evaporation technique. The transmittance of bio-nanocomposite films decreased with the increase of SNA content due to the formation of fewer agglomerates in the nanocomposite and light scattering at interface between SNA-rich and CL-rich phases. The thermal stability of CL/SNA nanocomposites was nearly similar to neat CL, even though the thermal property of SNA was inferior to neat CL. The tensile mechanical analysis exhibited that SNA did improve tensile strength and Young's module, however, a decrease of elongation at break at higher SNA loading levels (>5.0 wt%) in the present work. The thermal-mechanical analysis showed a good agreement with tensile mechanical analysis. Barrier properties of CL/SNA nanocomposite films showed that the addition of SNA led to an improvement of water vapor and oxygen permeability. For CL/SNA05, the nanocomposite film has relative high light transmittance (80% to neat CL film at 400 nm), improved Young's modulus and

tensile strength, and comparable elongation at break, favorable hydrophobicity (contact angle was 91°), and a higher gas barrier property (P<sub>O2</sub> and WVP decreased to 92% and 82.9% of CL film, respectively). By comparing the comprehensive properties of CL/SNA nanocomposites, SNA at the optimal 5.0 wt% loading level exhibited a higher reinforcing efficiency (higher Young's modulus and tensile strength, comparable elongation at break), improved WVP and P<sub>O2</sub>, and unchanged hydrophobicity.

### Acknowledgments

This work was supported by Program for Liaoning Excellent Talents in University (No. LJQ2012111), Social Development Plan of Liaoning Province (No.2012226013), and Chinese Nature Science Foundation (No. 51343002).

### Author Contributions

Fengyuan Huang designed the experiments; Xiaojie Wu and Yan Yu performed the experiments; Fengyuan Huang and Yanhua Lu wrote and revised the manuscript.

### Conflicts of Interest

The authors declare no conflict of interest.

### References

1. Filho, G.R.; Monteiro, D.S.; Meireles, C.S.; Nascimento de Assuncao, R.M.; Cerqueira, D.A.; Barud, H.S.; Ribeiro, S.J.L.; Messadeq, Y. Synthesis and characterization of cellulose acetate produced from recycled newspaper. *Carbohydr. Polym.* **2008**, *73*, 74–82.
2. Huang, F.Y. Thermal properties and thermal degradation of cellulose tri-stearate (CTs). *Polymers* **2012**, *4*, 1012–1024.
3. Kwatra, H.S.; Caruthers, J.M.; Tao, B.Y. Synthesis of long chain fatty acids esterified onto cellulose via the vacuum-acid chloride process. *Ind. Eng. Chem. Res.* **1992**, *31*, 2647–2651.
4. Crepy, L.; Miri, V.; Joly, N.; Martin, P.; Lefebvre, J.M. Effect of side chain length on structure and thermomechanical properties of fully substituted cellulose fatty esters. *Carbohydr. Polym.* **2011**, *83*, 1812–1820.
5. Granstrom, M.; nee Paakko, M.K.; Jin, H.; Kolehmainen, E.; Kilpelainen, I.; Ikkala, O. Highly water repellent aerogels based on cellulose stearoyl esters. *Polym. Chem.* **2011**, *2*, 1789–1796.
6. Crepy, L.; Monchau, F.; Chai, F.; Raoul, G.; Hivart, P.; Hildebrand, H.F.; Martin, P.; Joly, N. Evaluation of a bio-based hydrophobic cellulose laurate film as biomaterial—Study on biodegradation and cytocompatibility. *J. Biomed. Mater. Res. Part B Appl. Biomater.* **2012**, *100B*, 1000–1008.
7. Crépy, L.; Chaveriat, L.; Banoub, J.; Martin, P.; Joly, N. Synthesis of cellulose fatty esters as plastics—Influence of the degree of substitution and the fatty chain length on mechanical properties. *ChemSusChem* **2009**, *2*, 165–170.
8. Sealey, J.E.; Samaranayake, G.; Todd, J.G.; Glasser, W.G. Novel cellulose derivatives. IV. Preparation and thermal analysis of waxy esters of cellulose. *J. Polym. Sci. Part B Polym. Phys.* **1996**, *34*, 1613–1620.

9. Geissler, A.; Bonaccorso, E.; Heim, L.O.; Heinze, T.; Zhang, K. Temperature-responsive thin films from cellulose stearoyl triester. *J. Phys. Chem. C* **2014**, *118*, 2408–2417.
10. Dufresne, A. Crystalline starch based nanoparticles. *Curr. Opin. Colloid Interface Sci.* **2014**, *19*, 397–408.
11. Alexandre, M.; Dubois, P. Polymer-layered silicate nano-composites: Preparation, properties and uses of a new class of materials. *Mater. Sci. Eng. R Rep.* **2000**, *28*, 1–63.
12. Chakraborty, S.; Sahoo, B.; Teraoka, I.; Miller, L.M.; Gross, R.A. Enzyme-catalyzed regioselective modification of starch nanoparticles. *Macromolecules* **2005**, *38*, 61–68.
13. Thielemans, W.; Belgacem, M.N.; Dufresne, A. Starch nanocrystals with large chain surface modifications. *Langmuir* **2006**, *22*, 4804–4810.
14. Dufresne, A.; Cavaille, J.Y. Clustering and percolation effects in microcrystalline starch-reinforced thermoplastic. *J. Polym. Sci. Part B Polym. Phys.* **1998**, *36*, 2211–2224.
15. Angellier, H.; Molina-Boisseau, S.; Dufresne, A. Processing and structural properties of waxy maize starch nanocrystals reinforced natural rubber. *Macromolecules* **2005**, *38*, 9161–9170.
16. Chen, G.; Wei, M.; Chen, J.; Huang, J.; Dufresne, A.; Chang, P.R. Simultaneous reinforcing and toughening: New nanocomposites of waterborne polyurethane filled with low loading level of starch nanocrystals. *Polymer* **2008**, *49*, 1860–1870.
17. Angellier, H.; Molina-Boisseau, S.; Dole, P.; Dufresne, A. Thermoplastic starch—Waxy maize starch nanocrystals nanocomposites. *Biomacromolecules* **2006**, *7*, 531–539.
18. Garcia, N.L.; Ribba, L.; Dufresne, A.; Aranguren, M.I.; Goyanes, S. Physico-mechanical properties of biodegradable starch nanocomposites. *Macromol. Mater. Eng.* **2009**, *294*, 169–177.
19. Viguie, J.; Molina-Boisseau, S.; Dufresne, A. Processing and characterization of waxy maize starch films plasticized by sorbitol and reinforced with starch nanocrystals. *Macromol. Biosci.* **2007**, *7*, 1206–1216.
20. Kristo, E.; Biliaderis, C.G. Physical properties of starch nanocrystal-reinforced pullulan films. *Carbohydr. Polym.* **2007**, *68*, 146–158.
21. Yu, J.; Ai, F.; Dufresne, A.; Gao, S.; Huang, J.; Chang, P.R. Structure and mechanical properties of poly(lactic acid) filled with (starch nanocrystal)-graft-poly( $\epsilon$ -caprolactone). *Macromol. Mater. Eng.* **2008**, *293*, 763–770.
22. Chen, Y.; Cao, X.; Chang, P.R.; Huneault, M.A. Comparative study on the films of poly(vinyl alcohol)/pea starch nanocrystals and poly(vinyl alcohol)/native pea starch. *Carbohydr. Polym.* **2008**, *73*, 8–17.
23. Angellier, H.; Choisnard, L.; Molina-Boisseau, S.; Ozil, P.; Dufresne, A. Optimization of the preparation of aqueous suspensions of waxy maize starch nanocrystals using a response surface methodology. *Biomacromolecules* **2004**, *5*, 1545–1551.
24. LeCorre, D.; Dufresne, A.; Rueff, M.; Khelifi, B.; Bras, J. All starch nanocomposite coating for barrier material. *J. Appl. Polym. Sci.* **2014**, *131*, doi:10.1002/app.39826.
25. Namazi, H.; Dadkhah, A. Surface modification of starch nanocrystals through ring-opening polymerization of  $\epsilon$ -caprolactone and investigation of their microstructures. *J. Appl. Polym. Sci.* **2008**, *110*, 2405–2412.

26. Yano, H.; Sugiyama, J.; Nakagaito, A.N.; Nogi, M.; Matsuura, T.; Hikita, M.; Handa, K. Optically transparent composites reinforced with networks of bacterial nanofibers. *Adv. Mater.* **2005**, *17*, 153–155.
27. Nogi, M.; Iwamoto, S.; Nakagaito, A.N.; Yano, H. Optically transparent nanofiber paper. *Adv. Mater.* **2009**, *21*, 1595–1598.
28. Yang, Z.Y.; Wang, W.J.; Shao, Z.Q.; Zhu, H.D.; Li, Y.H.; Wang, F.J. The transparency and mechanical properties of cellulose acetate nanocomposites using cellulose nanowhiskers as fillers. *Cellulose* **2013**, *20*, 159–168.
29. Moon, R.J.; Martini, A.; Nairn, J.; Simonsen, J.; Youngblood, J. Cellulose nanomaterials review: Structure, properties and nanocomposites. *Chem. Soc. Rev.* **2011**, *40*, 3941–3994.
30. Li, X.; Qiu, C.; Ji, N.; Sun, C.; Xiong, L.; Sun, Q. Mechanical, barrier and morphological properties of starch nanocrystals-reinforced pea starch films. *Carbohydr. Polym.* **2015**, *121*, 155–162.
31. Mele, P.; Angellier-Coussy, H.; Molina-Boisseau, S.; Dufresne, A. Reinforcing mechanisms of starch nanocrystals in a nonvulcanized natural rubber matrix. *Biomacromolecules* **2011**, *12*, 1487–1493.
32. Vaca-Garcia, C.; Gozzelino, G.; Glasser, W.G.; Borredon, M.E. Dynamic mechanical thermal analysis transitions of partially and fully substituted cellulose fatty esters. *J. Polym. Sci. Part B Polym. Phys.* **2003**, *41*, 281–288.
33. Liu, D.; Zhong, T.; Chang, P.R.; Li, K.; Wu, Q. Starch composites reinforced by bamboo cellulosic crystals. *Bioresour. Technol.* **2010**, *101*, 2529–2536.
34. Kargarzadeh, H.; Sheltami, R.M.; Ahmada, I.; Abdullaha, I.; Dufresne, A. Toughened polyester cellulose nanocomposites: Effects of cellulose nanocrystals and liquid epoxidized natural rubber on morphology and mechanical properties. *Ind. Crops Prod.* **2015**, *72*, 125–132.
35. Aldana, D.S.; Villa, E.D.; de Dios Hernández, M.; Sánchez, G.G.; Cruz, Q.R.; Gallardo, S.F.; Castillo, H.P.; Casarrubias, L.B. Barrier properties of polylactic acid in cellulose based packages using montmorillonite as filler. *Polymers* **2014**, *6*, 2386–2403.
36. Condes, M.C.; Anon, M.C.; Mauri, A.N.; Dufresne, A. Amaranth protein films reinforced with maize starch nanocrystals. *Food Hydrocoll.* **2015**, *47*, 146–157.
37. Dou, Y.; Xu, S.; Liu, X.; Han, J.; Yan, H.; Wei, M.; Evans, D.G.; Duan, X. Transparent, flexible films based on layered double hydroxide/cellulose acetate with excellent oxygen barrier property. *Adv. Funct. Mater.* **2014**, *24*, 514–521.
38. Yang, Q.; Saito, T.; Isogai, A. Facile fabrication of transparent cellulose films with high water repellency and gas barrier properties. *Cellulose* **2012**, *19*, 1913–1921.